EASR

Engineering and Applied Science Research

https://www.tci-thaijo.org/index.php/easr/index

Published by the Faculty of Engineering, Khon Kaen University, Thailand

$(La^{3+}Mg^{2+})$ codoped $BiFeO_3$ nanopowders: Synthesis, characterizations, and giant dielectric relaxations

Pornsawan Kum-onsa[1)], Narong Chanlek[2)], Masaki Takesada[3)], Pornjuk Srepusharawoot[4, 5)] and Prasit Thongbai*[4, 5)]

[1)]Materials Science and Nanotechnology Program, Faculty of Science, Khon Kaen University, Khon Kaen 40002, Thailand
[2)]Synchrotron Light Research Institute (Public Organization), Nakhon Ratchasima 30000, Thailand
[3)]Department of Physics, Hokkaido University, Sapporo 060-0810, Japan
[4)]Department of Physics, Faculty of Science, Khon Kaen University, Khon Kaen 40002, Thailand
[5)]Institute of Nanomaterials Research and Innovation for Energy (IN-RIE), NANOTEC-KKU RNN on Nanomaterials Research and Innovation for Energy, Khon Kaen University, Khon Kaen 40002, Thailand

Received 15 March 2021
Revised 24 April 2021
Accepted 17 May 2021

Abstract

A new strategy to improve the dielectric properties of $BiFeO_3$ is proposed by codoping with La^{3+} and Mg^{2+} to control the ceramic microstructure and increase the dielectric permittivity (ε′), respectively. The main phase of $BiFeO_3$ is obtained in nanocrystalline powders of $La_xBi_{1-x}Fe_{1-x}Mg_xO_3$ (x = 0, 0.05 and 0.1), which are prepared by a chemical co-precipitation method. The particle size of the codoped $La_xBi_{1-x}Fe_{1-x}Mg_xO_3$ is smaller than that of the $BiFeO_3$. A dense ceramic microstructure without porosity is obtained by sintering at 800 °C for 3 h. The mean grain size of the $BiFeO_3$ ceramics decreases with increasing codoping (La^{3+}–Mg^{2+}) concentration. The primary roles of La^{3+} and Mg^{2+} are to suppress the grain growth and enhance the densification rate, respectively. At 1 kHz, the ε′ of the $La_xBi_{1-x}Fe_{1-x}Mg_xO_3$ with x = 0.1 increased significantly compared to that of the $BiFeO_3$, while the loss tangent (tanδ) was lower than that of the $BiFeO_3$. In addition, another role of Mg^{2+} is to increase the ε′ without any effect on the tanδ. Two dielectric relaxations are observed in low-frequency (150-250 K) and high-temperature (250-400 K) ranges. An X-ray photoelectron spectroscopy shows that the Fe^{2+}/Fe^{3+} ration in the codoped $La_xBi_{1-x}Fe_{1-x}Mg_xO_3$ increased compared to that of the $BiFeO_3$, corresponding to the increase in ε′. Thus, a low-temperature dielectric relaxation is attributed to the electron hopping between Fe^{2+}–O–Fe^{3+}. On the other hand, a high-temperature dielectric relaxation is caused by interfacial polarization relaxation.

Keywords: Dielectric permittivity, Dielectric relaxation, Electron hopping, Interfacial polarization

1. Introduction

In recent years, various kinds of giant dielectric materials such as Sr_2TiCrO_6 [1], $BaTiO_3$-0.5wt%$Na_{0.5}Bi_{0.5}TiO_3$ [2], Nd-doped $BaTiO_3$ [3], $La_{2-x}Sr_xNiO_4$ (LSNO) [4, 5], $CaCu_3Ti_4O_{12}$ (CCTO) [6-11], co-doped NiO [12], co-doped $SrTiO_3$ [13, 14], and co-doped TiO_2 [15-21] have been intensively investigated. These ceramic oxides can exhibit very high dielectric permittivity (ε′ ~ 10^3-10^5) in the radio-frequency range. Many research groups have focused on the potential applications of these ceramic oxides in electronic devices and studied the origin(s) of the giant dielectric response.

Although the loss tangent of many giant dielectric oxides is difficult to reduce and still higher than the standard level for practical applications, giant dielectric oxides have been intensively investigated to understand the underlying mechanism. The giant dielectric response in giant dielectric oxides is unlikely originated from the ferroelectric phase transition. Instead, the extrinsic mechanisms associated with the electron hopping and interfacial polarization are likely the primary cause [6, 12, 22-25]. Because of fascinating giant dielectric behaviors, the investigation of electrical and dielectric properties is still going on [6, 12, 26-30].

Generally, the sintering temperature of all giant dielectric oxides are very high. The sintering temperatures of the $SrTiO_3$-based, $La_{2-x}Sr_xNiO_4$, and co-doped TiO_2 ceramics are in the range of 1300-1550 °C [5, 12, 13, 15-17]. A giant dielectric oxide that can be fabricated by using a low temperature is a promising material for electronic industrials. $BiFeO_3$ ceramics can be prepared by using a low-temperature range. Interestingly, the $BiFeO_3$ ceramics can simultaneously show ferroelectric and (anti)ferromagnetic ordering [24, 31-35]. The dielectric permittivity of $BiFeO_3$ polycrystalline ceramics is lower than 200 at room temperature [36]. Interestingly, a high dielectric permittivity of ~10^3 can be obtained in $BiFeO_3$ ceramics by introducing Fe^{2+}/Fe^{3+} ions. The electrical response of the grain boundary and electron hopping between $Fe^{2+}\leftrightarrow Fe^{3+}$ ions may be the critical factors contributing to the overall dielectric responses in $BiFeO_3$ ceramics [33, 34].

*Corresponding author.
Email address: pthongbai@kku.ac.th
doi: 10.14456/easr.2021.79

According to the grain boundary response, the dielectric properties can be improved by controlling the microstructure. Reduced mean grain size to enhance the insulating grain boundary density is an effective method to suppress the leakage current and loss tangent. It was reported that the substitution of La^{3+} ions into $BiFeO_3$ ceramics could reduce the conductivity and loss tangent due to the reduction in the mean grain size [24, 37]. However, the reduced mean grain size of the La^{3+} single-doped $BiFeO_3$ ceramics is usually accompanied by residual pores in the ceramic microstructure. For many giant dielectric oxides, especially for CCTO ceramics, the substitution of Mg^{2+} into ceramics can increase the dielectric permittivity by retaining the loss tangent [38, 39]. Furthermore, Mg^{2+} can also enhance the densification rate of these giant dielectric oxides, giving rise to a dense ceramic microstructure. Thus, the substitution of La^{3+} and Mg^{2+} into $BiFeO_3$ ceramics could improve the microstructure and give important information on the origin of the giant dielectric properties.

Thus, this work aims to fabricate $BiFeO_3$-based oxides with enhanced dielectric permittivity and retaining low loss tangent. A new strategy to improve the dielectric properties of $BiFeO_3$ is proposed by codoping with La^{3+} and Mg^{2+} to control the ceramic microstructure and increase the ε', respectively. $La_xBi_{1-x}Fe_{1-x}Mg_xO_3$ powders nanocrystalline powders were synthesized using a chemical co-precipitation method. To obtain a dense ceramic microstructure, the compacted powders were sintered at 800 °C for 3 h. The dielectric properties were investigated over a wide temperature and frequency ranges and discussed in detail.

2. Materials and methods

2.1 Sample preparation

A co-precipitation method was used to prepare $La_xBi_{1-x}Fe_{1-x}Mg_xO_3$ powders, where x = 0, 0.05, and 0.1 to obtain nanocrystal line powders. The starting raw materials consisted of $Fe(NO_3)_3{\cdot}9H_2O$ (99.9%, KANTO), $MgN_2O_6{\cdot}H_2O$ (99%, Aldrich), $LaN_3O_9{\cdot}6H_2O$ (99%, Aldrich), $Bi(NO_3)_3{\cdot}5H_2O$ (99.9%, KANTO), nitric acid [HNO_3] (65%, ACI Labscan), poly(ethylene glycol) [PEG] ($M_w \sim 4000$, LABCHEM), and ammonia solution [NH_4OH] (28%, Qrec). First, the stoichiometric amounts of $Bi(NO_3)_3{\cdot}5H_2O$, $Fe(NO_3)_3{\cdot}9H_2O$, $MgN_2O_6{\cdot}H_2O$, and $LaN_3O_9{\cdot}6H_2O$ were weighed in proportion to the molar ratio for each composition (e.g., 3.2338 g of $Bi(NO_3)_3{\cdot}5H_2O$ and 2.6933 g of $Fe(NO_3)_3{\cdot}9H_2O$ for preparation of $BiFeO_3$) and mixed in deionized water (60 mL) with constant stirring at room temperature for 1 h. Second, 20 ml of HNO_3 were dissolved in this aqueous solution. Third, the solution was stirred until the orange transparent solution was observed. Next, PEG (2.6933 g) was added into the transparent solution, and then the temperature was increased to 60 °C with continuous stirring for 24 h. After that, 120 mL of NH_4OH was carefully dropped into the transparent solution until the precipitate solution was observed. Then, the precipitate solution was washed by deionized water until the pH of the solution was ~7 and was dried at 80 °C. The precursor powder was calcined at 600 °C for 3 h to obtain nanopowders. Finally, the compacted powders with a pellet shape were sintered in air at 800 °C for 3 h.

2.2 Sample characterization

The nanostructure particles of the calcined $La_xBi_{1-x}Fe_{1-x}Mg_xO_3$ powders were revealed using Focus Ion Beam-Field Scanning Electron Microscopy (FIB-SEM, FEI Helios NanoLab G3 CX). The phase formation and nanostructure of sintered $La_xBi_{1-x}Fe_{1-x}Mg_xO_3$ ceramics were analyzed using an X-ray Diffraction (XRD, PANalytical EMPYREAN). A scanning electron microscope (SEM) was used to reveal the ceramic microstructure of the sintered samples (SEC SNE-4500M). The chemical states of Fe were determined by X-ray photoelectron spectroscopy (XPS, PHI5000 VersaProbe II, ULVAC-PHI, Japan (at the SUT-NANOTEC-SLRI Joint Research Facility, Synchrotron Light Research Institute (SLRI), Thailand).

2.3 dielectric measurements

For dielectric measurements, the Ag paste was coated onto both sides of the sintered samples. The dielectric properties were tested in the frequency range of 10^2-10^7 Hz. In the temperature ranges of 0-300 K and 300-473 K, the measurements were performed using an Impedance Analyzer (KEYSIGHT E4990A) and Precision Impedance Analyzer (Agilent 4294A), respectively.

3. Results and discussion

The morphologies of the $La_xBi_{1-x}Fe_{1-x}Mg_xO_3$ powders prepared by a simple chemical co-precipitation method (calcined at 600 °C for 3 h) with different doping concentrations (x) are revealed in Figure 1(a-c). It was observed that the particle size of the BFO ceramics was remarkably reduced by co-doping with La^{3+} and Mg^{2+} ions. The particle size distribution is illustrated in Figure 1(d-f). The particle size of the BFO powder was estimated to be ~429 nm, while the particle sizes of the codoped $La_xBi_{1-x}Fe_{1-x}Mg_xO_3$ powders with x = 0.05 and 0.1 were reduced to be ~140 nm and ~182 nm, respectively. This result is similar to that reported in the literature [24, 37]. The reduction in the particle size is likely caused by the lattice strain due to the ionic size mismatch between the dopant and host ions.

The obtained nanocrystalline powders were compacted and sintered at 800 °C for 3 h for achieving the ceramic samples. The crystalline structure and phase compositions of the sintered ceramics were studied using the XRD technique. As shown in Figure 2, all the XRD patterns showed the main phase of $BiFeO_3$ with a rhombohedral perovskite structure (*R*3*c* space group, JCPDS 86-1518) [37, 40, 41]. However, the $Bi_{24}FeO_{40}$ and $Bi_2Fe_4O_9$ phases were also detected. The existence of these second phases was associated with the *evaporation of* Bi at elevated temperatures, leading to *nonstoichiometric compounds*. Thus, the second phases were formed during heating process. These impurities may have an influence on the microstructure of the co-doped $La_xBi_{1-x}Fe_{1-x}Mg_xO_3$ ceramics with x = 0.05 and 0.1.

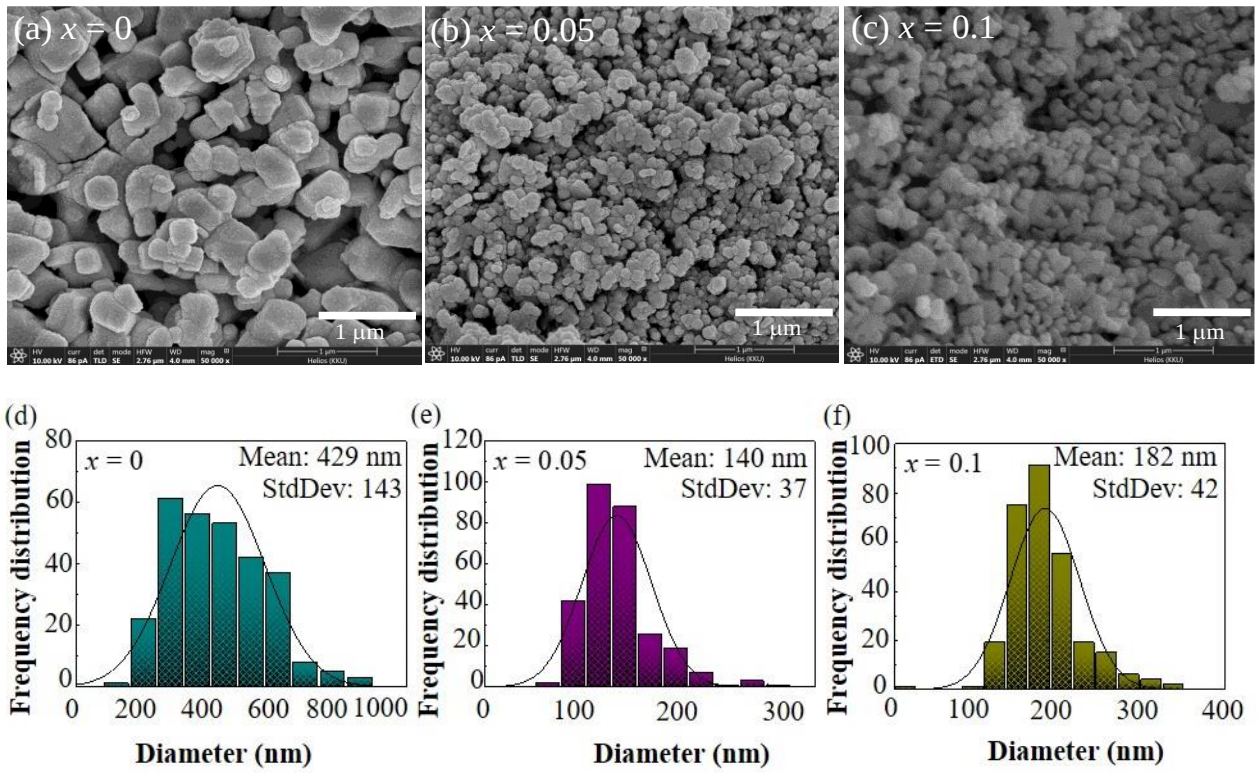

Figure 1 SEM Images of $La_xBi_{1-x}Fe_{1-x}Mg_xO_3$ powders with (a) $x = 0$, (b) $x = 0.05$ and (c) $x = 0.1$ powders. Particle size distribution of $La_xBi_{1-x}Fe_{1-x}Mg_xO_3$ powders with (d) $x = 0$, (e) $x = 0.05$ and (f) $x = 0.1$

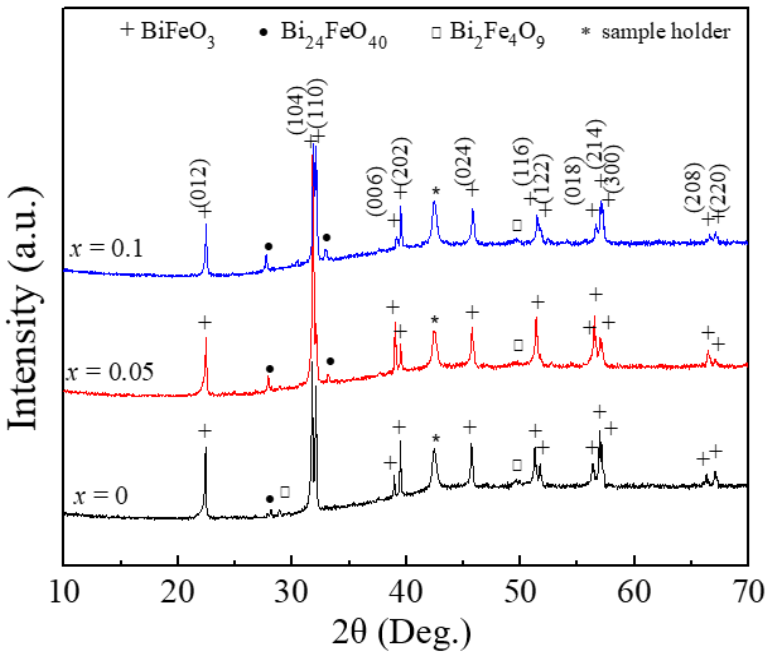

Figure 2 XRD Patterns of $La_xBi_{1-x}Fe_{1-x}Mg_xO_3$ ceramics with $x = 0$, 0.05 and 0.1

The oxidation states of an Fe element in the sintered ceramics were measured using the XPS technique. The XPS spectra of Fe2*p* for the $La_xBi_{1-x}Fe_{1-x}Mg_xO_3$ ceramics with $x = 0$, 0.05, and 0.1 are depicted in Figure 3. According to previous works, the variations of oxidation states (Fe^{2+}/Fe^{3+}) had an effect on the dielectric and electrical properties of $BiFeO_3$ ceramics due to the electron hopping between $Fe^{2+} \leftrightarrow Fe^{3+}$ sites [24, 25, 33]. As clearly shown in Figure 3, Fe^{2+} and Fe^{3+} ions were detected in all sintered ceramics, corresponding to the previous reports [25, 42, 43]. By fitting the XPS curves of all ceramics, the ratio of Fe^{2+}/Fe^{3+} can be obtained and found to be 61.96%, 63.53%, and 67.87% for the $La_xBi_{1-x}Fe_{1-x}Mg_xO_3$ ceramics with $x = 0$, 0.05, and 0.1, respectively. The Fe^{2+}/Fe^{3+} ratio slightly increased with increasing co-doping concentration. These results may be caused by the existence of oxygen vacancies during the sintering process. When oxygen releases from the lattice structure, free electrons have entered into Fe^{3+} ions, which was eventually changed to Fe^{2+}.

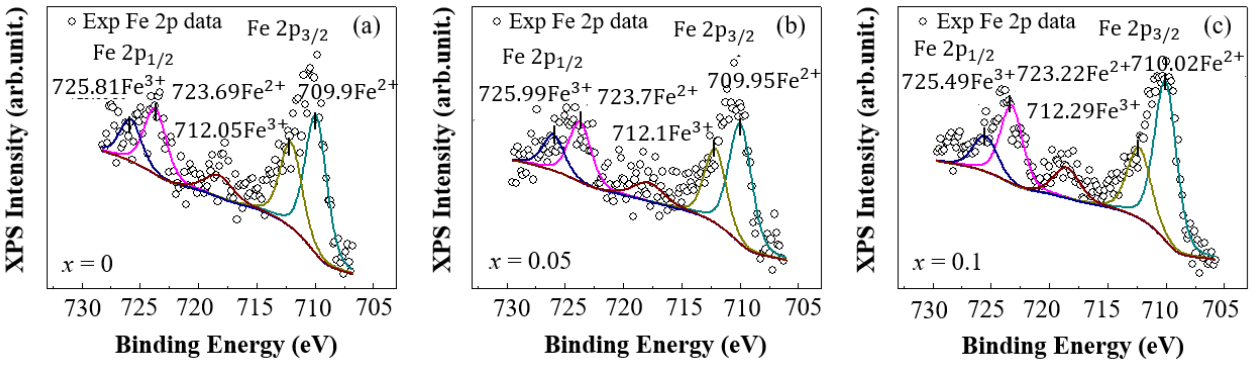

Figure 3 XPS Spectra of Fe2p for $La_xBi_{1-x}Fe_{1-x}Mg_xO_3$ ceramics with (a) $x = 0$, (b) $x = 0.05$ and (c) $x = 0.1$

The surface morphologies of the $BiFeO_3$ and codoped $La_xBi_{1-x}Fe_{1-x}Mg_xO_3$ ceramics, as well as the Mg^{2+} and La^{3+} single-doped $BiFeO_3$ ceramics, are illustrated in Figure 4. The grain size of $BiFeO_3$ ceramics is significantly decreased by doping with La^{3+} ions, Figure 4(d). However, many pores are observed in the ceramic microstructure. The grain size of the Mg^{2+} single-doped $BiFeO_3$ ceramic (Figure 4(e)) slightly reduces compared to that of the undoped $BiFeO_3$ ceramic (Figure 4(a)). These results are similar to that observed in the literature [24]. After substitution of Mg^{2+} into the La^{3+} single-doped $BiFeO_3$ ceramics with the same concentration for 5 at.% ($La_xBi_{1-x}Fe_{1-x}Mg_xO_3$ with $x = 0.05$), the ceramic microstructure was significantly changed. The microstructure of the $La_xBi_{1-x}Fe_{1-x}Mg_xO_3$ ceramic with $x = 0.05$ (Figure 4(b)) is similar to the undoped $BiFeO_3$ ceramic, indicating the dominant effect of Mg^{2+} doping ions on the enhanced grain growth of a $BiFeO_3$ ceramic. Notably, the microstructure of the $La_xBi_{1-x}Fe_{1-x}Mg_xO_3$ ceramic with $x = 0.1$ was highly dense with largely reduced grain size (Figure 4(c)). Thus, it can be suggested that the primary roles of La^{3+} and Mg^{2+} are to suppress the grain growth and enhance the densification rate, respectively. Furthermore, impurity particles in these samples can also inhibit grain growth rate. It is worth noting that the microstructures of the $La_xBi_{1-x}Fe_{1-x}Mg_xO_3$ ceramics with $x = 0$, 0.05, and 0.1 are highly dense without porosity. The dense microstructures of the $La_xBi_{1-x}Fe_{1-x}Mg_xO_3$ ceramics can be obtained by sintering at a relative low temperature compared to LSNO (~1400 °C) [5], CCTO (~1100 °C) [6, 7], co-doped NiO (~1200 °C) [12], and co-doped TiO_2 (~1400-1550 °C) [15, 16, 44].

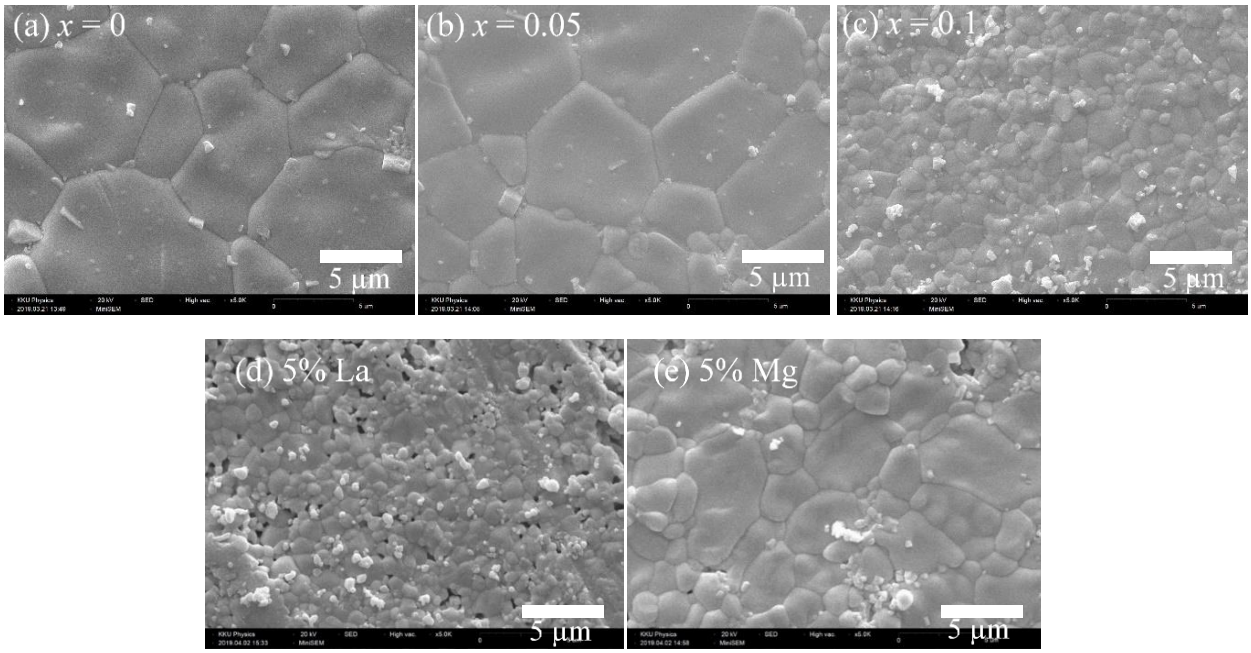

Figure 4 Surface morphologies of $La_xBi_{1-x}Fe_{1-x}Mg_xO_3$ ceramics with (a) $x = 0$, (b) $x = 0.05$, (c) $x = 0.1$, (d) 5%La doped-BiFeO3 and (e) 5%Mg doped BiFeO3

The dielectric properties at room temperature of the $La_xBi_{1-x}Fe_{1-x}Mg_xO_3$ ceramics, as well as the La^{3+} single-doped $BiFeO_3$ ceramic, are illustrated in Figure 5. The dielectric permittivity of all sintered ceramics suddenly decreases in a high-frequency range, corresponding to the observed loss tangent peak. This is the characteristic of the dielectric relaxation behavior [12, 25, 33]. The dielectric permittivity values at room temperature and 1 kHz for the La^{3+} single-doped $BiFeO_3$, $BiFeO_3$, and $La_xBi_{1-x}Fe_{1-x}Mg_xO_3$ ceramics with $x = 0.05$ and 0.1 are about 480, 4333, 4843, and 6256, respectively. The loss tangent values are 0.313, 0.229, 0.648, and 0.208, respectively. The dielectric permittivity of $BiFeO_3$ ceramics was decreased by doping with La^{3+} ions. After further codoping the La^{3+} single-doped $BiFeO_3$ ceramic with Mg^{2+}, the dielectric permittivity increased significantly, while the loss tangent also increased. Interestingly, with increasing the codoping concentration of La^{3+} and Mg^{2+}, the dielectric permittivity was significantly enhanced. Notably, the loss tangent was decreased. According to the XPS result, it is observed that the low-frequency dielectric permittivity of the $La_xBi_{1-x}Fe_{1-x}Mg_xO_3$ ceramics increases with increasing the Fe^{2+}/Fe^{3+} ratio. Obviously, the dielectric response at

room temperature of these ceramics should have partially resulted from the electron hopping between $Fe^{2+} \leftrightarrow Fe^{3+}$ ions. Codoping $BiFeO_3$ ceramic with La^{3+} and Mg^{2+} can cause an increase in the Fe^{2+}/Fe^{3+} ratio. Another reason is the effect of the grain boundary response. Doping Mg^{2+} into $BiFeO_3$ can increase the grain boundary capacitance [38], resulting in the enhanced dielectric permittivity. It is important to note that the loss tangent at 1 kHz of the $La_xBi_{1-x}Fe_{1-x}Mg_xO_3$ ceramic with $x = 0.1$ is the lowest. This result is correlated to its microstructure. As shown in Figure 4(c), the smallest grain size of the $La_xBi_{1-x}Fe_{1-x}Mg_xO_3$ ceramic with $x = 0.1$ reflects the largest density of the grain boundary layer, which is usually an insulating layer. Consequently, the DC conductivity in the $La_xBi_{1-x}Fe_{1-x}Mg_xO_3$ ceramic with $x = 0.1$ was decreased, giving rise to the decrease in the loss tangent.

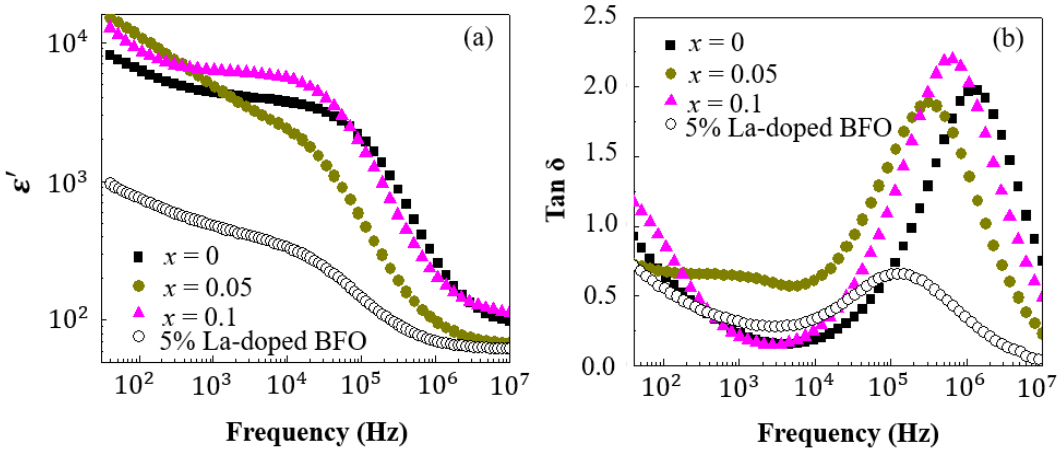

Figure 5 Dielectric properties at room temperature as a function of frequency for sintered $La_xBi_{1-x}Fe_{1-x}Mg_xO_3$ ceramics; (a) dielectric permittivity (ε′) and (b) loss tangent (tanδ)

To clearly clarify the effect of codopants on the dielectric relaxation behaviors, the dielectric properties as a function of frequency have been studied over a wide temperature range. As illustrated in Figure 6, the overall dielectric relaxation behaviors of all the samples are similar. Two dielectric relaxations are observed. The low-temperature dielectric relaxation exists in the temperate range of 150-250 K. The dramatic decrease in the dielectric permittivity is accompanied by the appearance of the loss tangent peak. Both the step-like decrease in the dielectric permittivity and the peak position of the loss tangent shift to higher temperatures as the frequency increased, indicating the thermally activated dielectric relaxation mechanism. The high-temperature relaxation behavior is observed in the temperature range of 250-400 K. This type of dielectric relaxation may be resulted from the interfacial polarization due to the accumulation of free changes at the internal interfaces. The relaxation peak of loss tangent can be observed in the low-temperature range only. Accordingly, the activation energy required for the relaxation process are 0.424, 0.554, and 0.436 eV for the $La_xBi_{1-x}Fe_{1-x}Mg_xO_3$ ceramics with $x = 0$, 0.05, and 0.1, respectively. The increased activation energy may be due to the fact that the electron hopping between $Fe^{2+} \leftrightarrow Fe^{3+}$ is inhibited by the dopants. Thus, the energy required for the relaxation process is increased. The dielectric permittivity in the temperature range below 150 K is lower than 100. The dielectric permittivity in such a low-frequency range is independent on frequency and temperature. This observation is resulted from the intrinsic polarization, i.e., dipolar and ionic polarizations.

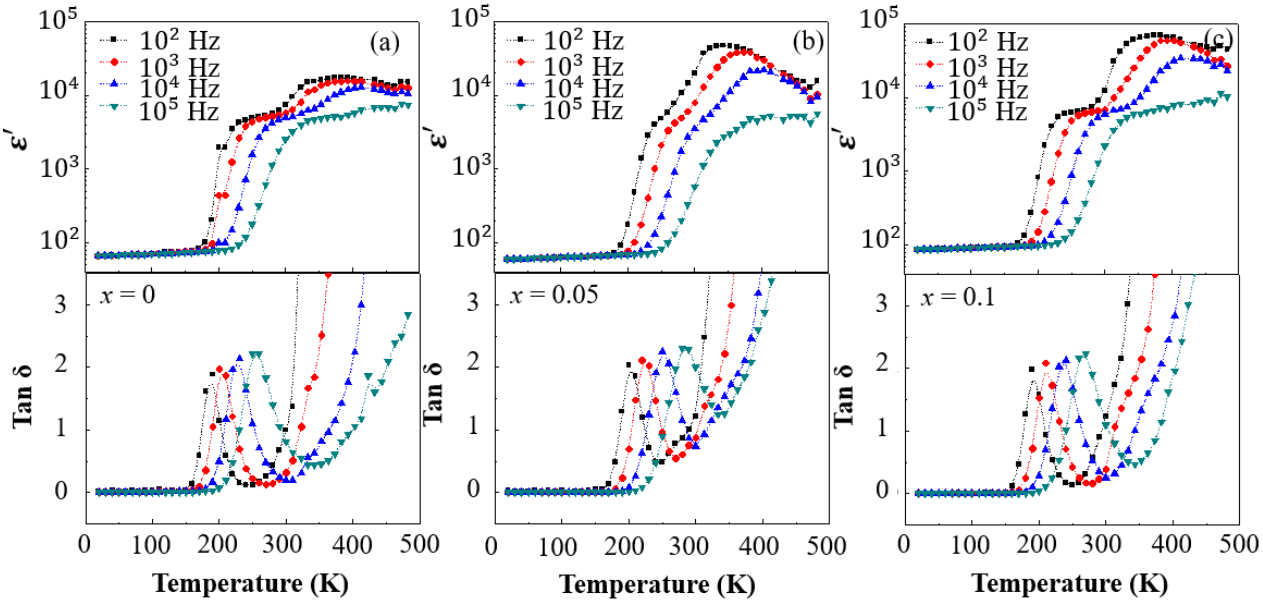

Figure 6 Temperature dependence of dielectric permittivity (ε′) and loss tangent (tanδ) at various frequencies for sintered $La_xBi_{1-x}Fe_{1-x}Mg_xO_3$ ceramics with (a) $x = 0$, (b) $x = 0.05$, (c) $x = 0.1$

4. Conclusions

We have prepared nanocrystal line powders of $La_xBi_{1-x}Fe_{1-x}Mg_xO_3$ with x = 0, 0.05, and 0.1 using a chemical co-precipitation method and calcined at 600 ˚C for 3 h. The particle size of $BiFeO_3$ ceramics was reduced by codoping with La^{3+} and Mg^{2+} ions. The microstructure of the sintered ceramics was highly dense without porosity. The mean grain size of the codoped $La_xBi_{1-x}Fe_{1-x}Mg_xO_3$ ceramics was greatly reduced by increasing the doping concentration. The existence of Fe^{2+} and Fe^{3+} ions were confirmed using the XPS technique. The Fe^{2+}/Fe^{3+} ratio slightly increased with increasing the codoping concentration. The dielectric permittivity of the La^{3+} doped-doped $BiFeO_3$ ceramic largely decreased compared to that of the $BiFeO_3$ ceramic. The dielectric permittivity of the La^{3+} doped-doped $BiFeO_3$ ceramic can be enhanced by further codoping with Mg^{2+}, while the loss tangent was lower than that of the $BiFeO_3$ ceramic. Substitution of Mg^{2+} ions can cause enhance the dielectric permittivity. The low- and high-temperature dielectric relaxations were observed in all sintered ceramics. The electron hopping between $Fe^{2+} \leftrightarrow Fe^{3+}$ and the interracial polarization were suggested to be the origin of these two dielectric responses, respectively.

5. Acknowledgements

This research was supported by the Basic Research Fund of Khon Kaen University and the Research and Graduate Studies, Khon Kaen University. P.K. would like to thank the Research and Graduate Studies, Khon Kaen University.

6. References

[1] Sun J, Ahmed R, Wang GJ, Wang ST, Wang J, Suhaib SA, et al. Colossal dielectric behavior and dielectric anomalies in Sr_2TiCrO_6 ceramics. J Mater Sci. 2019;54:6323-31.
[2] Wang W, Li L, Lu T, Wang R, Zhang N, Luo W, et al. Colossal permittivity in $BaTiO_3$-0.5wt%$Na_{0.5}Ba_{0.5}TiO_3$ ceramics with high insulation resistivity induced by reducing atmosphere. J Eur Ceram Soc. 2019;39(14):4168-76.
[3] Liu Q, Liu J, Lu D, Zheng W. Colossal dielectric behavior and relaxation in Nd-doped $BaTiO_3$ at low temperature. Ceram Int. 2018;44(6):7251-8.
[4] Park T, Nussinov Z, Hazzard K, Sidorov V, Balatsky A, Sarrao J, et al. Novel dielectric anomaly in the hole-doped $La_2Cu_{1-x}Li_xO_4$ and $La_{2-x}Sr_xNiO_4$ insulators: signature of an electronic glassy state. Phys Rev Lett. 2005;94:017002.
[5] Meeporn K, Yamwong T, Thongbai P. $La_{1.7}Sr_{0.3}NiO_4$ nanocrystalline powders prepared by a combustion method using urea as fuel: preparation, characterization, and their bulk colossal dielectric constants. Jpn J Appl Phys. 2014;53:06JF01.
[6] Adams T, Sinclair D, West A. Characterization of grain boundary impedances in fine- and coarse-grained $CaCu_3Ti_4O_{12}$ ceramics. Phys Rev B. 2006;73(9):094124.
[7] Felix AA, Saska LA, Bezzon VDN, Cilense M, Ramirez MA. Enhanced electrical behavior in $Ca_{1-x}Sr_xCu_3Ti_4O_{12}$ ceramics. Ceram Int. 2019;45:14305-11.
[8] Tang Z, Huang Y, Wu K, Li J. Significantly enhanced breakdown field in $Ca_{1-x}Sr_xCu_3Ti_4O_{12}$ ceramics by tailoring donor densities. J Eur Ceram Soc. 2018;38:1569-75.
[9] Chen K, Li GL, Gao F, Liu J, Liu JM, Zhu JS. Conducting grain boundaries in the high-dielectric-constant ceramic $CaCu_3Ti_4O_{12}$. J Appl Phys. 2007;101:074101.
[10] Liu L, Fan H, Wang L, Chen X, Fang P. Dc-bias-field-induced dielectric relaxation and ac conduction in $CaCu_3Ti_4O_{12}$ ceramics. Phil Mag. 2008;88:537-45.
[11] Yu R, Xue H, Cao Z, Chen L, Xiong Z. Effect of oxygen sintering atmosphere on the electrical behavior of CCTO ceramics. J Eur Ceram Soc. 2012;32:1245-9.
[12] Wu J, Nan CW, Lin Y, Deng Y. Giant dielectric permittivity observed in Li and Ti doped NiO. Phys Rev Lett. 2002;89:217601.
[13] Pan W, Cao M, Qi J, Hao H, Yao Z, Yu Z, et al. Defect structure and dielectric behavior in $SrTi_{1-x}(Zn_{1/3}Nb_{2/3})_xO_3$ ceramics. J Alloy Comp. 2019;784:1303-10.
[14] Pan W, Cao M, Diao C, Tao C, Hao H, Yao Z, et al. Structures and dielectric properties of (Nb, Zn) codoped $SrTiO_3$ ceramics at various sintering temperatures. J Mater Sci. 2019;54:12401-10.
[15] Tuichai W, Danwittayakul S, Chanlek N, Thongbai P. Nonlinear current-voltage and giant dielectric properties of Al^{3+} and Ta^{5+} codoped TiO_2 ceramics. Mater Res Bull. 2019;116:137-42.
[16] Hu W, Liu Y, Withers RL, Frankcombe TJ, Noren L, Snashall A, et al. Electron-pinned defect-dipoles for high-performance colossal permittivity materials. Nat Mater. 2013;12:821-6.
[17] Yang C, Wei X, Hao J. Colossal permittivity in TiO_2 codoped by donor Nb and isovalent Zr. J Am Ceram Soc. 2018;101: 307-15.
[18] Yu Y, Li WL, Zhao Y, Zhang TD, Song RX, Zhang YL, et al. Large-size-mismatch co-dopants for colossal permittivity rutile TiO_2 ceramics with temperature stability. J Eur Ceram Soc. 2018;38:1576-82.
[19] Hu W, Lau K, Liu Y, Withers RL, Chen H, Fu L, et al. Colossal dielectric permittivity in (Nb+Al) codoped rutile TiO_2 ceramics: compositional gradient and local structure. Chem Mater. 2015;27:4934-42.
[20] Liu GC, Fan HQ, Xu J, Liu ZY, Zhao YW. Colossal permittivity and impedance analysis of niobium and aluminum co-doped TiO_2 ceramics. Rsc Adv. 2016;6(54):48708-14.
[21] Wang X, Zhang B, Shen G, Sun L, Hu Y, Shi L, et al. Colossal permittivity and impedance analysis of tantalum and samarium codoped TiO_2 ceramics. Ceram Int. 2017;43:13349-55.
[22] Lunkenheimer P, Fichtl R, Ebbinghaus S, Loidl A. Nonintrinsic origin of the colossal dielectric constants in $CaCu_3Ti_4O_{12}$. Phys Rev B. 2004;70:172102.
[23] Thongbai P, Yamwong T, Maensiri S. Correlation between giant dielectric response and electrical conductivity of CuO ceramic. Solid State Comm. 2008;147:385-7.
[24] Yotburut B, Thongbai P, Yamwong T, Maensiri S. Electrical and nonlinear current-voltage characteristics of La-doped $BiFeO_3$ ceramics. Ceram Int. 2017;43:5616-27.
[25] Lin P, Cui S, Zeng X, Huang H, Ke S. Giant dielectric response and enhanced thermal stability of multiferroic $BiFeO_3$. J Alloy Comp. 2014;600:118-24.

[26] Ni L, Chen XM. Enhanced giant dielectric response in Mg-substituted $CaCu_3Ti_4O_{12}$ ceramics. Solid State Comm. 2009;149: 379-83.
[27] Wang CC, Zhang LW. Polaron relaxation related to localized charge carriers in $CaCu_3Ti_4O_{12}$. Appl Phys Lett. 2007;90:142905.
[28] Ni L, Chen XM. Dielectric relaxations and formation mechanism of giant dielectric constant step in $CaCu_3Ti_4O_{12}$ ceramics. Appl Phys Lett. 2007;91:122905.
[29] Kim CH, Jang YH, Seo SJ, Song CH, Son JY, Yang YS, et al. Effect of Mn doping on the temperature-dependent anomalous giant dielectric behavior of $CaCu_3Ti_4O_{12}$. Phys Rev B. 2012;85(24):245210.
[30] Zheng JC, Frenkel AI, Wu L, Hanson J, Ku W, Bozin ES, et al. Nanoscale disorder and local electronic properties of $CaCu_3Ti_4O_{12}$: an integrated study of electron, neutron, and x-ray diffraction, x-ray absorption fine structure, and first-principles calculations. Phys Rev B. 2010;81(14):144203.
[31] Nakashima S, Hayashimoto R, Fujisawa H, Shimizu M. Bulk photovoltaic effects in Mn-doped $BiFeO_3$ thin films and the optical strains. Jpn J Appl Phys. 2018;57(11S):11UF11.
[32] Okamoto N, Kariya K, Yoshimura T, Fujimura N. The effect of crystal distortion and domain structure on piezoelectric properties of $BiFeO_3$ thin films. Jpn J Appl Phys. 2018;57:11UF07.
[33] Hunpratub S, Thongbai P, Yamwong T, Yimnirun R, Maensiri S. Dielectric relaxations and dielectric response in multiferroic $BiFeO_3$ ceramics. Appl Phys Lett. 2009;94:062904.
[34] Wang QQ, Wang CC, Zhang N, Wang H, Li YD, Li QJ, et al. Dielectric relaxations in pure, La-doped, and (La, Co)-codoped $BiFeO_3$: post-sintering annealing studies. J Alloy Comp. 2018;745:401-8.
[35] Malik RA, Zaman A, Hussain A, Maqbool A, Song TK, Kim WJ, et al. Temperature invariant high dielectric properties over the range 200°C-500°C in $BiFeO_3$ based ceramics. J Eur Ceram Soc. 2018;38:2259-63.
[36] Dong G, Tan G, Liu W, Xia A, Ren H. Crystal structure and highly enhanced ferroelectric properties of (Tb, Cr) codoped $BiFeO_3$ thin films fabricated by a sol-gel method. Ceram Int. 2014;40:1919-25.
[37] Yotburut B, Yamwong T, Thongbai P, Maensiri S. Synthesis and characterization of coprecipitation-prepared La-doped BiFeO3 nanopowders and their bulk dielectric properties. Japanese J Appl Phys. 2014;53:06JG13.
[38] Boonlakhorn J, Putasaeng B, Kidkhunthod P, Thongbai P. Improved dielectric properties of (Y+Mg) codoped $CaCu_3Ti_4O_{12}$ ceramics by controlling geometric and intrinsic properties of grain boundaries. Mater Des. 2016;92:494-8.
[39] Boonlakhorn J, Kidkhunthod P, Thongbai P. A novel approach to achieve high dielectric permittivity and low loss tangent in $CaCu_3Ti_4O_{12}$ ceramics by codoping with Sm^{3+} and Mg^{2+} ions. J Eur Ceram Soc. 2015;35:3521-8.
[40] Vijayanand S, Mahajan MB, Potdar HS, Joy PA. Magnetic characteristics of nanocrystalline multiferroic $BiFeO_3$ at low temperatures. Phys Rev B. 2009;80:064423.
[41] Jalil MA, Chowdhury SS, Sakib MA, Yousuf SMEH, Ashik EK, Firoz SH, et al. Temperature-dependent phase transition and comparative investigation on enhanced magnetic and optical properties between sillenite and perovskite bismuth ferrite-rGO nanocomposites. J Appl Phys. 2017;122(8):084902.
[42] Gowrishankar M, Babu DR, Saravanan P. Room temperature multiferroism in La and Ti co-substituted $BiFeO_3$ nanoparticles. MaterLett. 2016;171:34-7.
[43] Lu YW, Qi X. Hydrothermal synthesis of pure and Sb-doped $BiFeO_3$ with the typical hysteresis loops of ideal ferroelectrics. J Alloy Comp. 2019;774:386-95.
[44] Dong W, Hu W, Berlie A, Lau K, Chen H, Withers RL, et al. Colossal dielectric behavior of Ga+Nb Co-doped rutile TiO_2. ACS Appl Mater Interfac. 2015;7(45):25321-5.